Controlling Spatial Distribution of Functional Lipids in a Supported Lipid Bilayer Prepared from Vesicles

Hyun-Su Lee,[*,†] *Ye Chan Kim,*[†] *Jacob S. Brenner,*[∥] *Vladimir R. Muzykantov,*[⊥] *Jacob W. Myerson,*[*,⊥] *and Russell J. Composto*[*,†,‡,§]

[†]Department of Materials Science and Engineering, [‡]Department of Chemical and Biomolecular Engineering, [§]Laboratory for Research on the Structure of Matter, [∥]Division of Pulmonary and Critical Care Medicine, [⊥]Department of Systems Pharmacology and Translational Therapeutics, University of Pennsylvania, Philadelphia, PA 19104, United States

Corresponding Authors

*E-mail: leeh1@seas.upenn.edu (H.S.L)

*E-mail: myerson@pennmedicine.upenn.edu (J.W.M.)

*E-mail: composto@seas.upenn.edu (R.J.C.)

KEYWORDS: supported lipid bilayer, quartz crystal microbalance, atomic force spectroscopy

ABSTRACT

Conjugating biomolecules, such as antibodies, to bioconjugate moieties on lipid surfaces is a powerful tool for engineering the surface of diverse biomaterials, including cells and nanoparticles. We developed supported lipid bilayers (SLBs) presenting well-defined spatial distributions of functional moieties as models for precisely engineered functional biomolecular-lipid surfaces. We used quartz crystal microbalance with dissipation (QCM-D) and atomic force microscopy (AFM) to determine how vesicles containing a mixture of 1,2-dipalmitoyl-sn-glycero-3-phosphatidylcholine (DPPC) and 1,2-distearoyl-sn-glycero-3-phosphoethanolamine-N-[azido(polyethylene glycol)-2000] (DSPE-PEG-N_3) form SLBs as a function of the lipid phase transition temperature (T_m). Above the DPPC T_m, DPPC/DSPE-PEG-N_3 vesicles form SLBs with functional azide moieties on SiO_2 substrates via vesicle fusion. Below this T_m, DPPC/DSPE-PEG-N_3 vesicles attach to SiO_2 intact. Intact DPPC/DSPE-PEG-N_3 vesicles on the SiO_2 surfaces fuse and rupture to form SLBs when temperature is brought above the DPPC T_m. AFM studies show uniform and complete DPPC/DSPE-PEG-N_3 SLB coverage of SiO_2 surfaces for different DSPE-PEG-N_3 concentrations. As the DSPE-PEG-N_3 concentration increases from 0.01 to 6 mol%, the intermolecular spacing of DSPE-PEG-N_3 in the SLBs decreases from 4.6 to 1.0 nm. The PEG moiety undergoes a mushroom to brush transition as DSPE-PEG-N_3 concentration varies from 0.1 to 2.0 mol%. Via copper-free click reaction, IgG was conjugated to SLB surfaces with 4.6 nm or 1.3 nm inter-DSPE-PEG-N_3 spacing. QCM-D and AFM data show; 1) uniform and complete IgG layers of similar mass and thickness on the two types of SLB; 2) a higher-viscosity/less rigid IgG layer on the SLB with 4.6 nm inter-DSPE-PEG-N_3 spacing. Our studies provide a blueprint for SLBs modeling spatial control of functional macromolecules on lipid surfaces, including surfaces of lipid nanoparticles and cells.

1. INTRODUCTION

Supported lipid bilayers (SLB) are a simple and robust model system for investigating the behavior of lipid membranes, such as cell or lipid nanoparticle surfaces. Surface-functionalized SLBs have been used to characterize multiple single molecule-scale phenomena of biological interest, including viral interactions,[1-7] protein-protein interactions,[8,9] antibody-antigen interactions,[10,11] and substrate-enzyme complexes.[12,13] As examples, angiotensin-converting enzyme II (ACE2) receptor was embedded in SLBs to study SARS-CoV-2 binding to and infection of cells[5,14-16] and ganglioside GM1 SLBs have been used for biosensors that detect cholera toxin B and monitor amyloid-beta 40 aggregation.[17]

In targeted medicine studies, the surfaces of lipidic nano- and microparticles have been modified with functional molecules that confer targeting or therapeutic effects.[18-21] Our recent work indicates that immune responses to protein-coated nanoparticle surfaces are sensitive to the spatial arrangement of the surface-presented protein.[22-24] In the present study, we develop methods for preparing SLBs that can serve as a model platform for investigating biomacromolecule-functionalized lipidic particle surfaces where we precisely control the spatial distribution of surface moieties.

Studies of SLB formation mainly focus on how lipid vesicles convert into SLBs on hydrophilic surfaces, as a function of key parameters such as electrostatic interactions, temperature, and solvent, as well as buffer solutions.[25-37] SLB studies use techniques such as quartz crystal microbalance with dissipation monitoring (QCM-D), atomic force microscopy (AFM), and neutron reflection.[26-28] Here, we use QCM-D and AFM to prepare SLBs from vesicles made of DPPC, previously studied in the SLB literature, and DSPE-PEG-N_3, a functional lipid allowing us

to use our SLBs to model bioconjugate reactions on lipid surfaces. To modulate the spatial distribution of protein conjugation moieties on SLBs, the DSPE-PEG-N_3 concentration in the mixed-lipid vesicles was set as 0, 0.01, 0.1, 1, 2 or 6 mol%. QCM-D studies show that DPPC/DSPE-PEG-N_3 vesicles form SLBs on SiO_2 substrates when $T \geq T_m$ of DPPC. When $T < T_m$, the vesicles stably deposit on SiO_2. Using the Sauerbrey relation[38-47] and a Voigt-based viscoelastic model[40-47] to analyze the QCM-D results, we find the mol% of DSPE-PEG-N_3 in the SLB is greater than that in the original vesical incorporated in the SLBs. As the concentration of DSPE-PEG-N_3 in the vesicle increases from 0.01 to 6 mol%, the distance between DSPE-PEG-N_3 lipids in the SLBs decreases from ~5 nm to ~1 nm and the thickness of PEG moiety increases from ~1.3 nm to ~5.5 nm. We find the PEG moiety undergoes a mushroom to brush transition as DSPE-PEG-N_3 concentration varies from 0.1 to 2.0 mol%. Via copper-free click chemistry, IgG was conjugated to SLB surfaces with 4.6 nm and 1.3 nm inter-DSPE-PEG-N_3 spacing. QCM-D and AFM show that the resultant IgG layers are uniform and have similar mass density and thickness, but the IgG layer on SLB with 4.6 nm inter-DSPE-PEG-N_3 spacing has a higher viscosity/more flexibility, showing that spatial arrangement of functional moieties on a lipid surface can selectively change properties of a biomolecular layer grafted onto the lipid surface. These studies show that SLBs with precisely controlled functional group arrangement can interrogate interactions between proteins and lipid surfaces. Our SLB platform may be used to optimize the structure of functional biomaterials surfaces.

2. EXPERIMENTAL SECTION

2.1. Materials

QCM-D sensor crystals, AT-cut piezoelectric quartz crystals (14 mm in diameter and 0.3 mm thickness) coated with silicon oxide (SiO_2, 50 nm) and gold (Au, 100 nm) Promimic AB, were purchased from Biolin Scientific, USA. N-Type (100) oriented silicon wafers (CZ silicon, dopant; Ph, 20−30 Ω resistivity) were purchased from Silicon Quest International. 1,2-dipalmitoyl-sn-glycero-3-phosphatidylcholine (99%, DPPC, phase transition temperature = 41 °C), Egg yolk l-α-phosphatidylcholine (egg PC, phase transition temperature ~ -15 °C), and 1,2-distearoyl-sn-glycero-3-phosphoethanolamine-N-[azido(polyethylene glycol)-2000] (DSPE-PEG-N_3, M_w of PEG = 2000 g/mol) were purchased from Avanti Polar Lipids (Alabaster, AL), respectively. Thiol-end-functionalized polyethylene glycol (HS-PEG-2K; M_n = 2000 g/mol) was purchased as monodisperse (M_w/M_n = 1.05) sample from Polymer Source, Inc. (Dorval, Canada). For buffer preparation, sodium chloride (99.5%) was purchased from ThermoFisher. Water used throughout this study was purified with a milli-Q water purification system (Millipore, Molsheim, France).

2.2. *In-situ* QCM-D

A QCM instrument (Model E4, Q-Sense Inc., Gothenburg, Sweden) capable of dissipation monitoring was used to quantify lipid adsorption on SiO_2 surfaces. Mass of material in aqueous suspension deposited on SiO_2 surfaces was determined via measurement of piezoelectric quartz crystal resonance frequencies. The Sauerbrey equation relates the change in the resonant frequency to the change in mass deposited on the quartz crystal,[38-47]

$$\Delta m = -C\frac{\Delta f_n}{n}$$

Where C is the mass sensitivity constant (C = 17.7 ng $cm^{-2}Hz^{-1}$ for an AT-cut, 5 MHz crystal) and n is the vibrational mode number (n = 1, 3, 5, 7,). The dissipation change, ΔD_n, indicates physical

characteristics of the deposited layer such as viscosity and elasticity. If ΔD_n is less than 2.0×10^{-6} and the plots of $\Delta f_n/n$ over time for several modes superimpose, the adsorbed layer behaves like an elastic solid and mass of the elastic layer was calculated using the Sauerbrey equation.[38-47] If ΔD_n is greater than 2.0×10^{-6}, the adsorbed layer behaves like a viscoelastic gel composed of the macromolecules and the coupled solvent. Therefore, the Sauerbrey equation is not accurate for determining dry mass. However, physical properties (thickness, shear modulus, and viscosity) of the absorbed layer were estimated by best fitting the QCM-D experimental data ($\Delta f_n/n$ *(n=3,5,7)* and ΔD_n) with a Voigt-based viscoelastic model using Q-tools software accompanying the apparatus (Q-Sense Inc),[38-47] as shown in Figure S1, S3, S5, and S9, Supporting information (SI). SiO_2-coated and gold-coated QCM sensor crystals were cleaned by exposing to UV-Ozone for 20 minutes, followed by immersing in 95% ethanol for 30 minutes at room temperature, rinsing with ultrapure water (Millipore Direct-Q, 18 mΩ cm resistivity), drying with N_2 (g), and re-exposing to UV-Ozone for 20 minutes to remove organic and biological impurities. Control experiments were performed to study azide-functionalized PEG (M_w = 2000 g/mol) layers formed on SLBs (DPPC+DSPE-PEG-N_3). Here, we exposed the gold coated QCM sensor surface to a dilute solution (35 μM) of HS-PEG-2K in DI water at 21 °C (flow rate = 20 μL/min). The thiol functional group is well-known to coordinate strongly to gold at room temperature to form highly grafted polymer brushes on gold surfaces.[40,41] QCM-D results for grafting HS-PEG-2K to gold are shown in Figure S1 and Table S1, Supporting information (SI). To study the formation of SLB, QCM-D studies were performed using silicon oxide surface sensors. We used a 100 mM NaCl solution as the baseline diluent, egg PC vesicle solutions (0.125 mg/mL) with 2 mol% and 0 mol% DSPE-PEG-N_3, and DPPC vesicle solutions (0.125 mg/mL) with 6 mol%, 2 mol%, 1 mol%, 0.1 mol%, 0.01 mol%, and 0 mol% DSPE-PEG-N_3. The liquid medium was circulated by peristaltic pump at

a rate of 20 µL/min through a flow cell containing the sensor crystal. The temperature of the system was maintained between 21 °C and 50 °C, with temperature programs for different conditions, including annealing of surface-bound intact lipid vesicles, described in the results section. Lastly, IgG deposition studies were performed by exposing the blended SLBs formed using 0.01 mol% and 1.0 mol% DSPE-PEG-N_3 to DBCO (20×) to an IgG solution (0.124 mg/mL) at 30 °C (flow rate = 10 µL/min), followed by rinsing with 100 mM NaCl.

The mol%, distance, and APL of DSPE-PEG-N_3 in the blended lipid bilayer were determined in the following manner. The area per lipid (APL) of pure DPPC SLB, defined as the cross-sectional area of the whole system along the bilayer surface plane, divided by half the total number of lipids present in the bilayer,[48] was estimated using the QCM-D measured deposited mass of pure DPPC SLB, with an assumption that the mole number of lipids is identical in the bottom and top layers of the bilayers. This outcome is similar to the computationally efficient prediction of area per lipid (APL) of DPPC lipid bilayer at 320 K (APL = 0.567 nm^2).[48,49] Our calculation of APL assumes that DSPE-PEG-N_3 deposition on the lower leaflets of the supported lipid bilayers will be negligible due to steric hindrance (Figure 3(a)). The lower leaflets of the mixed lipid bilayers, containing only DPPC per the first assumption, will be identical to the lower leaflets of the pure DPPC bilayers. Another assumption is that the packing density of lipid tails will be identical in the pure DPPC layers versus the mixed lipid layers, with only the arrangement of DSPE-PEG-N_3 in the layers changing. Details regarding the assumptions and analytical methods for converting QCM measurements of deposited mass to APL and lipid spacing values are found in the supporting information (Table S4, Figure S10).

2.3. Atomic force microscopy (AFM)

Silicon wafers (5 mm × 5 mm for AFM measurements) were cleaned by immersion in piranha solution (3:1 (v:v) H_2SO_4/30% H_2O_2 (Fisher Scientific)), rinsed with ultrapure water (Millipore Direct-Q, 18 MΩ cm resistivity), dried with N_2, and exposed to UV–ozone to produce an homogeneous hydroxylated surface and to remove impurities. For AFM measurements, each lipid bilayer deposition on silicon oxide surfaces (cleaned silicon waters; 5 mm × 5 mm) was performed by immersion of the wafers into DPPC vesicle solutions (0.125 mg/mL) with 1 mol%, 0.01 mol%, and 0 mol% DSPE-PEG-N_3 at 50 °C, followed by rising with 100 mM NaCl solutions, similar to treatments in QCM-D experiments. Each IgG deposition on silicon oxide surfaces (cleaned silicon waters; 5 mm × 5 mm) was performed by immersion of the blended SLBs on wafers formed using with 1.0 mol%, 0.01 mol%, and 0 mol% DSPE-PEG-N_3 into DBCO (20×) IgG solutions (0.124 mg/mL) at 30 °C, followed by rinsing with 100 mM NaCl solutions, similar to treatments in QCM-D experiments.

Surface topography and morphology were determined by atomic force microscopy (Dimension Icon AFM, Bruker). A probe with a spring constant of 40 N/m, a radius of curvature of about 8 nm, and a resonance frequency of approximately 325 kHz was used in tapping mode. AFM images were taken over a scan size of 1 μm × 1 μm. Images were analyzed using Gwyddion software.

2.4. Lipid Vesicle Preparation

Lipid mixtures of egg PC, DPPC, and DSPE-PEG-N_3 (Avanti), with compositions defined in the text of the results, were prepared in chloroform, dried under nitrogen gas, then lyophilized overnight. Dried lipids were resuspended in 100 mM NaCl in MilliQ water to a total lipid concentration of 2.5 mg/mL by vortexing until a homogeneous suspension was achieved. The suspensions were bath sonicated for 50 minutes at 40°C. After sonication, the suspensions were

subjected to three freeze-thaw cycles, with three minutes in liquid nitrogen followed by three minutes sonication at 40°C for each cycle. The formed vesicles were syringe extruded by hand through 50 nm cutoff track-etched polycarbonate filters eleven times at 50°C.[50] Hydrodynamic diameters of the vesicles were assessed by DLS (Malvern), with diameters of 100 nm ± 15 nm taken as standards for use of the vesicles. Vesicle concentrations were checked with nanoparticle tracking analysis (Malvern) and vesicle concentrations of 2-3 × 10^{12} vesicles per mL were prepared for use in QCM-D and AFM experiments.

2.5. DBCO-IgG Preparation

Whole rat IgG (ThermoFisher) was conjugated to dibenzocyclooctyne-PEG(4)-N-Hydroxysuccinimide ester (DBCO-NHS, Jena Bioscience) to confer reactivity to azide-terminated lipids. IgG solutions in phosphate-buffered saline were incubated with DBCO-NHS for one hour at room temperature at a molar ratio of 1(IgG):20(DBCO-NHS). DBCO-NHS that did not conjugate to the IgG was separated from the solution by centrifugation against 10 kDa cutoff filters (Amicon) in five wash-filtration cycles. After recovery of IgG-DBCO conjugates, efficiency of the reaction was assessed via optical absorbance spectra. Absorbance peaks at 280 nm and 309 nm indicated concentrations of IgG and DBCO, respectively. Overlap between the DBCO and IgG spectra was accounted for by $Abs_{280,corrected} = Abs_{280} - 1.089 \times Abs_{309}$. IgG concentration was calculated as $[IgG] = Abs_{280,corrected}/\varepsilon_{280,IgG}$ where $\varepsilon_{280,IgG}$ is the IgG extinction coefficient for 280 nm light, 204000 L*mol^{-1}cm^{-1}. DBCO concentration was calculated as $[DBCO] = Abs_{309}/\varepsilon_{309,DBCO}$ where $\varepsilon_{309,DBCO}$ is the DBCO extinction coefficient for 309 nm light, 12000 L*mol^{-1}cm^{-1}. Average DBCO:IgG molar ratio was determined as the ratio of the above concentrations and DBCO-functionalized IgG was used in QCM and AFM studies if the yield DBCO:IgG was between 11 and 15.

2.6. Differential Scanning Calorimetry

Vesicles prepared from egg PC, egg PC+2.0 mol% DSPE-PEG-N_3, DPPC, and DPPC+2.0 mol% DSPE-PEG-N_3 were analyzed with differential scanning microcalorimetry, to assess the thermal properties of the vesicles and confirm the phase transition temperature of the DPPC and DPPC+2.0 mol% DSPE-PEG-N_3 vesicles. Lipid vesicles suspensions in 100 mM NaCl were prepared at 0.25 mg/mL total lipid concentration. The same 100 mM NaCl solution used to prepare and dilute the vesicles was used as a reference solution. The lipid vesicle suspensions and reference solutions were heated from 4°C to 100°C at 1°C per minute in a TA Instruments Nano DSC operating in scanning mode. Background measurements of reference 100 mM NaCl vs. reference 100 mM NaCl were subtracted from all thermograms obtained for lipid vesicles vs. reference solutions. Using TA Instruments NanoAnalyze software, a sigmoidal fit was applied to the baseline for all background-subtracted thermograms, in order to identify phase transition temperatures, enthalpy change of phase transitions, and entropy changes of phase transitions.

3. RESULTS AND DISCUSSION

3.1. Deposition of Egg PC and Egg PC blended with DSPE-PEG-N_3 on SiO_2

To construct SLBs with azide(N_3)-functionalized surfaces for QCM-D experiments, we first used egg PC, a lipid mixture studied previously.[25-27] Vesicles were prepared from egg PC blended with 0.0 mol% and 2.0 mol% DSPE-PEG-N_3 (PEG; M_w = 2000 g/mol). Vesicle deposition on silicon oxide surfaces was studied *in situ* using QCM-D at 21°C (T > egg PC T_m ~ -15°C). Using differential scanning microcalorimetry, we confirmed that the egg PC and egg PC/2.0 mol% DSPE-PEG-N_3 vesicles had melting temperatures below 4°C (Figure S2, SI). After using 100 mM NaCl solution to establish a baseline, SiO_2-coated QCM crystal sensors were exposed to both

vesicle solutions (arrow 1 in Figure 1). After vesicle exposure, $\Delta f_n/n$ $(n=3)$ and ΔD_n rapidly decrease and increase, respectively, over about 150 sec. Steady state is reached after about 12.5 min of exposure. Rinsing with 100 mM NaCl solution (arrow 2 in Figure 1) does not affect the values of $\Delta f_n/n$ $(n=3)$ and ΔD_n. For egg PC vesicles without DSPE-PEG-N_3, the final values of $\Delta f_n/n$ $(n=3)$ and ΔD_n are −24 Hz and 0.3×10^{-6}, respectively. This outcome is similar to the characteristic frequency and dissipation changes previously reported for egg PC deposition at 21°C on SiO_2 surfaces.[25-27] In that work, these changes were attributed to vesicle adsorption and fusion, followed by lipid spreading to form SLBs on SiO_2 surfaces.[26] Therefore, the QCM-D results indicate that our egg PC vesicles formed thin and elastic lipid bilayers on SiO_2 surfaces. For egg PC blended with 2.0 mol% DSPE-PEG-N_3, the final values of $\Delta f_n/n$ $(n=3)$ and ΔD_n were -45 Hz and 2.4 x 10^{-6}, respectively (Figure 1, blue curves). Thus, the addition of DSPE-PEG-N_3 to egg PC yielded SLBs with $\Delta f_n/n$ $(n=3)$ and ΔD_n values that were lower and higher, respectively, than those for egg PC alone, indicating that the hydrated PEG groups on DSPE-PEG-N_3 increase the surface-deposited mass and the viscoelasticity of the mixed lipid layer (Figure 1, lower panel inset, blue arrow).[51]

The thickness of the SLBs formed from egg PC was determined by modeling the QCM-D results ($\Delta f_n/n$ $(n=3,5,7)$ and ΔD_n) with the Voigt-based viscoelastic model (Figure S3(a) and S3(b), Table S2, SI).[40-47] Egg PC and egg PC with 2.0 mol% DSPE-PEG-N_3 form SLB layers of 5.2 nm and 9.8 nm thickness, respectively, on SiO_2. This difference in thickness suggests that the azide-PEG tether adds ~4.6 nm to the egg PC with DSPE-PEG-N_3. The radius of gyration (R_g) of free PEG (M_w = 2000 g/mol) is 1.5 nm.[52,53] Thus, the PEG groups in the egg PC+DSPE-PEG-N_3 SLBs are likely in an extended conformation greater than R_g of free PEG, corresponding to the brush regime.[51]

Subsequent studies with DPPC+DSPE-PEG-N_3 SLBs support the conclusion that PEG in SLBs with 2.0 mol% DSPE-PEG-N_3 does indeed take on a brush conformation (Figure 3).

Egg PC is an interesting real world lipid system. However, its complexity limits the quantitative analysis of QCM-D results. Egg PC contains a mixture of acyl chains with 16 to 22 carbon atoms and varying numbers of double bonds, which confounds analysis of the deposited molecules. Additionally, the Sauerbrey equation does not accurately determine deposited mass for dissipation changes greater than 2.0×10^{-6}.[38-42] Due to the complexity of the egg PC mixture and its "viscoelastic" properties, we did not estimate the mol% DSPE-PEG-N_3 incorporated into the egg PC+DSPE-PEG-N_3 SLBs, the area per DSPE-PEG-N_3 lipid (APL), and the average distance between DSPE-PEG-N_3 lipids. Instead, the following sections detail the validation of dipalmitoyl phosphatidylcholine (DPPC)+DSPE-PEG-N_3 SLBs as a model system for creating SLBs where detailed analysis and control of nanoscale parameters is feasible.

3.2 Deposition of DPPC and DPPC blended with DSPE-PEG-N_3 on SiO_2

DPPC was chosen as a model lipid to fabricate SLBs because DPPC has a long history of use in nanomedicines and exhibits has a high phase transition temperature (T_m = 41 °C) that favors a more stable and rigid SLBs. Taking advantage of this high transition temperature, experiments with DPPC and DPPC blended with DSPE-PEG-N_3 were performed across a range of temperatures below and above T_m = 41 °C.

3.2.1. Deposition of Pure DPPC and DPPC/DSPE-PEG-N_3 at 21°C ($T < T_m$)

QCM-D was used to monitor the deposition of DPPC vesicles containing 0.0 mol%, 0.01 mol%, 0.1 mol%, 1.0 mol%, 2.0 mol%, or 6.0 mol% DSPE-PEG-N_3 on SiO_2 surfaces at 21 °C under 20 µL/min flow (Figure 2a). For all systems, the frequency and dissipation change begin after ~10

min (arrow 1) as shown in Figure 2a. For pure DPPC, frequency decreases and dissipation increase slowly over ~50 minutes before reaching plateau values of -75 Hz and 10.5 × 10^{-6}, respectively (Figure 2a, black curves). Similar results were reported in the literature for DPPC deposition on SiO_2 at 25°C with a flow rate of 100 μL/min.[33] The protracted and large changes in both frequency and dissipation factor are characteristic of vesicle adsorption and fusion to form lipid bilayers, followed by additional attachment of intact lipid vesicles on top of the bilayer. After rinsing with 100 mM NaCl (black arrow 2), $\Delta f_n/n$ *(n=3)* and ΔD_n remain constant, indicating that the bilayer plus intact vesicle structure forms a stable viscoelastic layer under these flow conditions.

Upon adding 0.01 mol% DSPE-PEG-N_3 to DPPC vesicles, the frequency decreases and dissipation increases slowly over ~50 minutes and reach plateau values at -85 Hz and *8.5* × 10^{-6} at 20 μL/min flow at 21°C (Figure 2a, red curves). These results indicate that the surface structure is similar to that formed by pure DPPC vesicles on SiO_2. However, unlike the pure DPPC case, rinsing with 100 mM NaCl results in $\Delta f_n/n$ *(n=3)* increasing by 5 Hz and ΔD_n *(n=3)* decreasing by 1.0 × 10^{-6}. This indicates removal of the intact DPPC+0.01 mol% DSPE-PEG-N_3 lipid vesicles attached on the top of lipid bilayer. This "weaker" attachment may be attributed to PEG tethers interfering with the interactions between the vesicles and the underlying bilayer, as shown in the leftmost inset in Figure 2a.[51]

Increasing DSPE-PEG-N_3 to 0.1 mol%, 1.0 mol%, 2.0 mol%, or 6.0 mol% (Figure 2a, blue/pink/green/purple curves) induces changes in lipid assembly on SiO_2 surfaces at 21°C under 20 μL/min flow. First, these vesicles reach steady state frequency and dissipation changes within 10 minutes of exposure to SiO_2, compared to ~50 minutes for DPPC vesicles with 0 or only 0.01 mol% DSPE-PEG-N_3. Unlike the 0.01 mol% DSPE-PEG-N_3 case, the frequency and dissipation of DPPC vesicles with high DSPE-PEG-N_3 content are unaffected by rinsing (Figure 2a, top panel,

arrow 2). DPPC vesicles with 0.1 mol%, 1.0 mol%, 2.0 mol%, or 6.0 mol% DSPE-PEG-N_3 achieve final frequency values of -60 Hz, -80 Hz, -90 Hz, and -98 Hz and final dissipation values of 2.0×10^{-6}, 3.0×10^{-6}, 3.0×10^{-6}, and 3.2×10^{-6}, respectively. The frequency results indicate that the mass deposited at 21°C increases as DSPE-PEG-N_3 content in the vesicles increases. The dissipation values and deposition times suggest deposition of intact vesicles on the SiO_2 surface without SLB formation, as shown in Figure 2a (bottom panel, lower right inset). Unlike with the pure DPPC vesicle or those with only 0.01 mol% DSPE-PEG-N_3, the higher concentration of PEG-terminated lipids appears to stabilize the DPPC/DSPE-PEG-N_3 vesicle, preventing fusion, rupture, and formation of lipid bilayers. The final dissipation values for vesicles with high DSPE-PEG-N_3 content are smaller than for low-DSPE-PEG-N_3 vesicles, indicating that the layer of intact high-DSPE-PEG-N_3 vesicles on SiO_2 is less viscoelastic than the low-DSPE-PEG-N_3 intact vesicle layers adsorbed on top of SLBs. This behavior agrees with literature findings for layers of intact vesicles on gold or titanium oxide surfaces.[26-28,34]

3.2.2. Deposition of Pure DPPC and DPPC/DSPE-PEG-N_3 at 50°C ($T > T_m$)

For $T > T_m = 41$°C, DPPC vesicles can form lipid bilayers on negatively charged surfaces by adsorption, fusion, and rupture.[33] Our differential scanning calorimetry measurements confirm that vesicles of pure DPPC vesicles and DPPC with 2.0 mol% DSPE-PEG-N_3 have phase transition temperatures of 41°C (Figure S4, SI). To create a supported lipid bilayer that can be a platform for attaching proteins, we repeated the above QCM-D studies with DPPC/DSPE-PEG-N_3 vesicles at 50°C. As shown in Figure 2b, DPPC/DSPE-PEG-N_3 deposition at 50°C yielded lower frequency and dissipation changes than deposition at 21°C (Figure 2a, Figure S5, SI). These low frequency and dissipation changes are consistent with vesicle adsorption, fusion, and spreading to form a SLBs. The low dissipation values (below 2.0×10^{-6}) and superimposed plots of $\Delta f_n/n$ over time

for several modes (*n=3,5,7*), as shown in Figure S5, correspond to thin and rigid layers, sufficiently elastic for valid application of the Sauerbrey equation.[34-43] For qualitative and mass analyses of QCM-D data collected at high temperature (above 40 °C), $\Delta f_n/n$ and ΔD_n *of* frequency mode number 7 (*n=7*) were used because they showed more consistent plots (without noise peak) than those of other frequency mode numbers (*n=3,5*).

For DPPC/DSPE-PEG-N_3 deposition at 50°C, the changes in frequency, $\Delta f_n/n$ *(n=7),* and dissipation, ΔD_n, reach steady state values ~10 minutes after SiO_2 exposure to vesicles. For all DPPC/DSPE-PEG-N_3 compositions, rinsing with 100 mM NaCl solution after lipid deposition did not change $\Delta f_n/n$ *(n=7)* and ΔD_n values (Figure 2b, arrow 2). For 0.0 mol%, 0.01 mol%, 0.1 mol%, 1.0 mol%, 2.0 mol%, or 6.0 mol% DSPE-PEG-N_3 (Figure 2b, black/red/blue/pink/green/purple curves), the final frequency values were -25.1 Hz, -25.8 Hz, -29.7 Hz, -34.7 Hz, -37.9 Hz, and -44.9 Hz, respectively, indicating increased surface-deposited mass with increasing DSPE-PEG-N_3 content in the vesicles. The final dissipation values were 0.3×10^{-6}, 0.82×10^{-6}, 1.65×10^{-6}, 1.66×10^{-6}, 1.66×10^{-6}, and 1.79×10^{-6}, suggesting slightly increased viscoelasticity as more hydrated PEG is introduced to the deposited material.

The pure DPPC SLB characteristics at 50 °C were determined from QCM-D analysis (Table 1). The total deposited mass of the SLB was determined using the Sauerbrey equation[38-47] The thickness of the SLB was determined using the Voigt-based viscoelastic model (Figure S5, SI).[40-47] For the pure DPPC SLB, the area per lipid (APL) and thickness are 0.54 nm^2 and 4.5 nm (Table S4, SI), respectively, matching values previously reported for computational modeling of SLBs.[48,49] The DPPC SLB was thinner than the egg PC SLB (average thickness = 5.2 nm at 21 °C), suggesting DPPC SLBs are more homogeneous and stable at high temperature.

Table 1 also shows the mol% of DSPE-PEG-N_3 within the DPPC/DSPE-PEG-N_3 SLBs, the APL of DSPE-PEG-N_3, and the average distance between DSPE-PEG-N_3 lipids, as estimated from the deposited masses of the mixed lipid layers, compared to measurements for pure DPPC layers. Details regarding the calculation method are found in supporting information (Table S4, Figure S10). The mol % of DSPE-PEG-N_3 increases from 1 to 28 as the concentration of DSPE-PEG-N_3 increases from 0.01 to 6 mol% in bulk vesicles (before deposition). As DSPE-PEG-N_3 in the SLB increases, the intermolecular spacing and APL of DSPE-PEG-N_3 decrease, with the intermolecular spacing approaching a value of ~1 nm (Table 1, Figure 3b black curve).

For DPPC SLBs formed from vesicles containing 0.0 mol%, 0.01 mol%, 0.10 mol%, 1.0 mol%, 2.0 mol%, and 6.0 mol% DSPE-PEG-N_3, the final thicknesses are 4.5 nm, 5.8 nm, 6.0 nm, 8.5 nm, 9.7 nm, and 10.0 nm, respectively (Table 1). Correspondingly, the thickness of the azide-end-functionalized PEG layer increases by 1.3 nm, 1.5 nm, 4.0 nm, 5.2 nm, and 5.5 nm (Figure 3b red curve).

We propose that as the mol% of DSPE-PEG-N_3 increases, the PEG chains are forced to be closer to one another, provoking conformational extension of the PEG tether and a brush structure, as shown in Figure 3. To quantify this transition, the reduced tethered density ($\Sigma = \sigma \pi R_g^2$)[54] of PEG chains was estimated using the grafting density ($\sigma = 1/l^2$) of DSPE-PEG-N_3 (PEG, M_w = 2000) within the SLBs and the radius of gyration (R_g = 1.5 nm) of free PEG (M_w = 2000)[52,53] (Table 1). For 1.3 mol% DSPE-PEG-N_3, the chain-to-chain distance (l) between PEG groups is 4.6 nm, which is greater than twice the R_g of the free PEG chain (~3 nm). For this concentration of DSPE-PEG-N_3, the PEG thickness added to the SLB is 1.3 nm, approximately matching R_g[52,53]. This finding suggests that PEG chains do not overlap with their neighboring chains. Correspondingly, Σ is 0.3 chains (σ = 0.05 chains/nm^2) (Table 1, Figure 3 (b)), corresponding to

the mushroom regime ($\Sigma < 1$).[54] Thus, PEG in the SLBs extends to approximately R_g. Between 8.3 mol% and 19.0 mol% DSPE-PEG-N_3, Σ of the PEG chains increases from 2.2 to 4.9 chains (Table 1. Figure 3 (b)), corresponding to the mushroom-to-brush transition regime ($1 < \Sigma < 5$).[54] For the highest loading of DSPE-PEG-N_3 (28.1 mol%), *l* of PEG is 0.98 nm. For this case, *l* is much less than $2R_g$ (~3 nm) and the PEG thickness added to the SLB (5.5 nm) is much greater than R_g (~1.5 nm), consistent with stretching of the PEG chain. Here, Σ is 7.4 chains (σ = 1.04 chains/nm^2) (Table 1, Figure 3 (b)), corresponding to the brush regime ($5 < \Sigma$).[54] Overall, these results suggest that the mol% DSPE-PEG-N_3 and average distance between DSPE-PEG-N_3 lipids in the SLB, and therefore the grafting density, can be controlled by varying the mol% of DSPE-PEG-N_3 in the lipid vesicles. Further, by controlling the brush-brush spacing parameters the extension of PEG chains from the SLB can be tuned, which is important for subsequent attachment of biomolecules.

To further investigate PEG conformation, we grafted HS-PEG (M_w = 2000) directly to a gold surface. For this case where PEG is unable to diffuse, the reduced tethered density (Σ) and thickness values are 12.8 chains (σ = 1.81 chains/nm^2) and 8.3 nm, respectively (Table S1, SI) which represents a highly stretched brush.[54] Compared to this control study, the grafting density and the thickness of PEG chains in the fluid-like SLB case are reduced. This difference between characteristics of a covalently bound brush and a mobile brush within a fluid SLB requires further study.

To further examine the SLBs formed at 50 °C, DPPC vesicles containing 0.0 mol%, 0.01 mol%, and 1.0 mol% DSPE-PEG-N_3, were deposited at 50 °C on silicon oxide. The surface morphology, root mean square roughness (R_{rms}), and phase of dry SLBs were characterized using tapping mode AFM (Figure 4). After verifying that the underlying silicon oxide surfaces were smooth and

homogeneous (Figure 4a), the SLBs formed on silicon oxide surfaces yielded AFM images and R_{rms} values (Figure 4b-d) distinguishable from the silicon oxide prior to vesicle exposure (Figure 4a, R_{rms} = 0.20 ± 0.05 nm), indicating that the SLB is uniform and homogeneously distributed across the substrate. Figures 4c and 4d show similar height and phase images for the blended SLBs formed using 0.01 mol% and 1.0 mol%, DSPE-PEG-N_3, respectively, indicating that the PEG-terminated lipids are uniformly distributed across the mixed-lipid SLBs. Relative to the pure DPPC SLB (R_{rms} = 0.22 ± 0.03 nm, Figure 4b), the R_{rms} values for the blended SLBs increase to 0.27 ± 0.04 nm and 0.27 ± 0.04 nm, respectively, indicating surface roughness increase due to the PEG groups in the mixed-lipid SLBs.

3.2.3. Transition from intact vesicles to supported lipid bilayers via temperature change

The above results show that DPPC/DSPE-PEG-N_3 vesicles form the desired SLBs on SiO_2 at temperatures above the T_m of DPPC (50 °C > 41 °C), but deposit as intact vesicles at temperatures below the T_m (21 °C < 41 °C). Below, we describe studies in which intact DPPC/DSPE-PEG-N_3 vesicles are deposited at 21 °C, and then heat-treated between 21 °C and 50 °C to drive an *in situ* transition from attached vesicles to SLBs (Figure S6, SI). After establishing a baseline at 21 °C, SiO_2-coated QCM crystal sensors were exposed to DPPC vesicle solutions containing 2.0 mol% or 6.0 mol% DSPE-PEG-N_3 to form a layer of intact vesicles as in Figure 2a. The temperature of was increased to 50 °C over 30 minutes and then lowered to 21 °C. The values of $\Delta f_n/n$ *(n=7)* and ΔD_n previously observed at 21 °C were similar to the intact vesicle depositions depicted in Figure 2a. After the 21 °C → 50 °C → 21 °C annealing (Figure S6, SI), the final values of $\Delta f_n/n$ *(n=7)* and ΔD_n are consistent with those measured for SLBs formed at 50 °C, as depicted in Figure 2b. Therefore, these results are consistent with a transition from deposited intact vesicles to supported lipid bilayers induced by *in situ* heat treatment.

Figure 5 shows a plot of $\Delta f_n/n$ $(n=7)$ versus temperature for surfaces coated with initially intact DPPC vesicles prepared with 2.0 mol% or 6.0 mol% DSPE-PEG-N_3. In the absence of DSPE-PEG-N_3, the $\Delta f_n/n$ $(n=7)$ and ΔD_n increase linearly with temperature, due to the temperature dependence of the viscosity and density of the 100 mM NaCl buffer (Figure S7, Table S3, SI). In contrast, for samples containing DSPE-PEG-N_3, $\Delta f_n/n$ $(n=7)$ increases non-linearly with temperature, exhibiting sharper increases between 40 to 42°C and ~42 to 45°C for 6.0 mol% and 2.0 mol%, respectively. Thus, the dependence of frequency change on increasing temperature can be divided into three regimes: Sub-transition temperature (regime I); Transition temperature (regime II); Supra-transition temperature (regime III). $\Delta f_n/n$ $(n=7)$ exhibits a weak dependence on temperature in Regime I, indicating only temperature-dependent changes in the viscosity and density of intact vesicles on the SiO_2 surfaces. Regime II is characterized by a steep increase in the $\Delta f_n/n$ $(n=7)$ vs. temperature slope, indicating rupturing of vesicles that form the SLB (Figure 5, Table S3, SI). In regime III, the $\Delta f_n/n$ $(n=7)$ vs. temperature slope decreases again, indicating temperature-dependent changes in the viscosity and density of a stable DPPC/ DSPE-PEG-N_3 lipid bilayer (Figure 5, Table S3, SI). For the intact vesicles, the transition from regime I to II starts near 40°C and 44°C for mixtures prepared from 6.0 and 2.0% DSPE-PEG-N_3, respectively. These transitions are near the T_m of DPPC (41°C), indicating that the melting of the DPPC component of the intact vesicles enables the transition from intact vesicle to SLB. Moreover, the lower transition temperature for the 6.0 DSPE-PEG-N_3 system suggests that the incorporation of DSPE-PEG-N_3 reduces the stability of the intact vesicles. Taken together with the findings of section 3.2.2, this data shows that mixed-lipid vesicles can form mixed-lipid SLBs on surfaces either by deposition at $T > T_m$ or by deposition of intact vesicles at $T < T_m$, followed by annealing of the

vesicle layers at $T > T_m$, where T_m corresponds to the phase transition temperature for the lipids (Figure S6, S7, S8, Table S3, SI).

3.3. DBCO-functionalized IgG grafting to azide-functionalized SLBs

Bio-orthogonal copper-free click chemistry has been used to conjugate biomacromolecules to various surfaces, including lipid particles like liposomes.[22] Rat IgG was functionalized with strained alkyne (dibenzocyclooctyne/DBCO) for conjugation to DPPC/DSPE-PEG-N_3 SLBs, mimicking conjugation to liposomes. Using vesicles made from DPPC, DPPC+0.01 mol% DSPE-PEG-N_3, and DPPC+1.0 mol% DSPE-PEG-N_3, SLBs were prepared at 50 °C on SiO_2-coated QCM crystal sensors. The pure DPPC and azide-end functionalized SLBs were exposed to DBCO-IgG solutions (0.124 mg/mL) at 30 °C under 10 µL/min flow. For pure DPPC SLBs with no DBCO-reactive groups, $\Delta f_n/n$ $(n=3)$ and ΔD_n $(n=3)$ are zero (Table 2), indicating no non-specific adsorption of DBCO-IgG on SLBs without DBCO-azide reactions.

QCM-D results for DBCO-functionalized IgG grafting to azide-functionalized SLBs are shown in Figure 6a. For the mixed SLB containing 1.3 mol% DSPE-PEG-N_3, $\Delta f_n/n$ $(n=3)$ and ΔD_n $(n=3)$ decrease and increase, respectively, and then approach a steady state value after ~60 minutes of exposure to DBCO-IgG (Figure 6a, solid line). For the SLB containing 15.2 mol% of DSPE-PEG-N_3, $\Delta f_n/n$ $(n=3)$ and ΔD_n $(n=3)$ decrease and increase, respectively, and approach a steady state value after ~180 minutes exposure to DBCO-IgG (Figure 6a, dashed-dot line). For the 1.3 mol% and 15.2 mol% DSPE-PEG-N_3 cases, the final values for $\Delta f_n/n$ $(n=3)$ (-21 Hz and -23 Hz) and ΔD_n $(n=3)$ (1.8×10^{-6} and 0.7×10^{-6}), respectively, suggest chemically grafted DBCO-IgG layers that increase the viscoelasticity of the SLBs, relative to the deposited SLBs. Rinsing with 100 mM NaCl caused $\Delta f_n/n$ $(n=3)$ and ΔD_n $(n=3)$ to *slightly* increase and decrease, respectively (Figure 6a,

Arrow 2). This behavior can be attributed to a small quantity of physisorbed DBCO-IgG being removed from the SLBs. For pure DPPC SLBs, $\Delta f_n/n$ $(n=3)$ and ΔD_n $(n=3)$ are zero (Table 2), indicating very little non-specific adsorption of DBCO-IgG on SLBs without DSPE-PEG-N_3.

Thickness and viscosity of the grafted IgG layers were obtained by fitting $\Delta f_n/n$ $(n=3,5,7)$ and ΔD_n to the Voigt-based viscoelastic model (Figure 6b-c, Table 2, Figure S9, SI).[40-47] Thickness vs. time for DBCO-IgG grafting to DPPC/DSPE-PEG-N_3 SLBs (Figure 6b) mirrors $\Delta f_n/n$ vs. time (Figure 6a). The DBCO-IgG layer thickness is similar (~4 nm) for the 1.3 mol% and 15.2 mol% DSPE-PEG-N_3 SLBs. However, the maximum thickness is achieved 3× faster for the SLB with the lower grafting density of DSPE-PEG-N_3. DBCO-IgG attachment to 1.3 mol% DSPE-PEG-N_3 SLBs results in films that are 5.6× more viscous vs. IgG layers grafted to 15.2 mol% DSPE-PEG-N_3 SLBs (Figure 6c).

IgG grafting depends on the presentation of the DSPE-PEG-N_3 lipid in the SLB. At low grafting density (1.3 mol% DSPE-PEG-N_3), the azide attachment points are 4.6 nm apart (Table 1) and the PEG brush is in a mushroom conformation. As shown in schematic Figure 7a, DBCO-IgG is more likely to be grafted via one azide group, resulting in loosely tethered protein and a greater viscosity change. At high grafting density (15.2 mol% DSPE-PEG-N_3), we hypothesize that each DBCO-IgG is more likely to react with multiple azide groups in the SLB. The higher DSPE-PEG-N_3 density results in closer spacing, 1.3 nm, between azide groups and an extended PEG-N_3 brush, as shown in schematic Figure 7b. Attachment of each DBCO-IgG to multiple azides would account for the longer reaction time for DBCO-IgG interaction with the SLBs (see Figure 6). Crosslinking of DBCO-IgG to multiple azides would result in a more tightly-bound IgG layer, accounting for the smaller viscosity change when grafting to the SLB containing 15.2 mol% DSPE-PEG-N_3.

Finally, tapping mode AFM assessed the surface morphology, root mean square roughness (R_{rms}), and phase of DBCO-IgG layers grafted onto azide-end-functionalized SLBs containing 1.3 mol% and 15.2 mol% DSPE-PEG-N_3 (Figure 8). SLBs were prepared on SiO_2 at 50°C and DBCO-IgG was grafted to the SLBs at 30°C. As a control, DBCO-IgG was exposed to a pure DPPC SLB. The resulting AFM images (Figure 8a, $R_{rms} = 0.22 \pm 0.04$ nm) are indistinguishable from the DPPC SLB prior to DBCO-IgG exposure (Figure 4b, $R_{rms} = 0.22 \pm 0.03$ nm), indicating minimal non-specific DBCO-IgG adsorption. By contrast, DBCO-IgG exposure to SLBs containing azide-terminated lipids yielded AFM images and R_{rms} values (Figure 8b-c) distinguishable from the azide-end-functionalized SLBs prior to DBCO-IgG exposure ($R_{rms} = 0.27 \pm 0.04$ nm in Figure 4c; $R_{rms} = 0.27 \pm 0.04$ nm in Figure 4d), indicating successful grafting of the DBCO-IgG. Relative to the DBCO-IgG layer on the 1.3 mol% DSPE-PEG-N_3 SLB ($R_{rms} = 1.42 \pm 0.34$ nm, Figure 8b), the R_{rms} value of the DBCO-IgG attached to the 15.2 mol% DSPE-PEG-N_3 SLB decreases ($R_{rms} = 1.07 \pm 0.24$ nm, Figure 8c), consistent with a more tightly-bound IgG layer that is cross linked to DSPE-PEG-N_3 via multiple azide sites. Phase profiles for the DBCO-IgG layers were similar for the two tested SLBs. The similar distribution of IgG is consistent with the QCM studies that found similar thickness values for the two concentrations of DSPE-PEG-N_3.

Conclusion

Our recent studies of complement, often the first immune response to foreign surfaces like those of protein-coated nanoparticles, demonstrate that surface protein arrangement can modulate the immune response to a surface. In fact, we have shown sensitivity of complement C3 deposition to antibody spacing on IgG-grafted lipid nanoparticle surfaces.[22-24] Noting the emerging relevance of surface structure of functional coatings to the engineering of biomaterials, we designed this work to contribute to the improved control and characterization of the structure of functionalized

surfaces. The present study demonstrates a unique approach for manipulating and characterizing the spatial arrangement of functional moieties in SLBs. SLBs were formed on SiO_2 from DPPC/DSPE-PEG-N_3 vesicles either by driving vesicle rupture and fusion above the melting temperature of DPPC or by depositing intact vesicles on the surface below the melting temperature, and then annealing the surface-bound vesicles above the melting temperature. Using QCM-D data and analysis, SLBs were modeled to determine the molar density of DSPE-PEG-N_3 in the SLBs and the average spacing of functional DSPE-PEG-N_3 lipids. We show that increasing the composition of DSPE-PEG-N_3 in the vesicle results in an increase in DSPE-PEG-N_3 found in the SLBs, with the DSPE-PEG-N_3 concentration in the SLB being greater than that in the original vesicle. As the molar density of DSPE-PEG-N_3 in the SLBs was increased, the intermolecular spacing of DSPE-PEG-N_3 lipids decreased from 4.6 nm to 1 nm. The reduced DSPE-PEG-N_3 spacing leads to conformational extension of the PEG tether, corresponding to a transition from a mushroom structure to a brush conformation. AFM data confirm the homogeneity and uniformity of DPPC/DSPE-PEG-N_3 SLBs. We demonstrate that our SLBs with controlled spatial arrangement of functional moieties can be used as anchors for IgG, a functional biomacromolecule. IgG with strained alkyne groups was grafted onto SLBs containing 1.3 mol% and 15.2 mol% DSPE-PEG-N_3. IgG layers on the two SLBs have similar densities, but the closer spacing of azide groups in the 15.2 mol% DSPE-PEG-N_3 SLB appears to allow IgG to bridge multiple azide anchor points. As a result, IgG layers are more rigidly attached (i.e. lower viscosity) vs. IgG layers grafted on SLBs with lower grafting density (1.3 mol% DSPE-PEG-N_3). Therefore, this study shows that varying the spatial arrangement of functional moieties presented by SLBs controls physical properties of functional biomacromolecule layers built on the SLBs. In total, our studies show how to synthesize and characterize SLBs with controlled spatial arrangement of functional moieties,

promising SLBs that model cell or lipid particle surfaces presenting layers of functional molecules where we control the physical properties of functional molecule layers built on the lipid surface. We anticipate that future studies with such SLBs can provide insights into the design and study of the physical properties of functionalized lipid particles and surfaces. We plan further studies investigating immune protein responses to our SLBs, where we hope to determine how the spatial arrangement of surface-presented protein (IgG and other moieties) affects the interactions of blood proteins with lipid coatings.

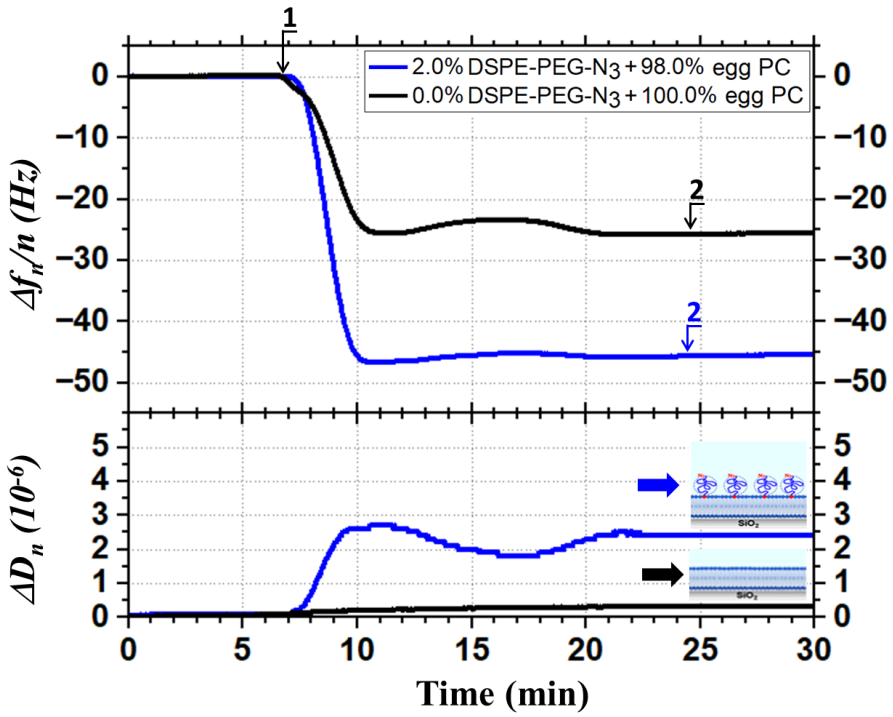

Figure 1. Traces of *$\Delta f_n/n$ (n=3) and ΔD_n (n=3)* vs. time for exposure of silicon oxide-coated crystal to egg PC (black curves) or egg PC + 2.0 mol% DSPE-PEG-N_3 (blue curves) vesicle solutions at 21 °C (flow rate = 20 µL/min). 100 mM NaCl was used for each baseline (*$\Delta f_n/n$ (n=3) and ΔD_n* = 0). Each vesicle solution was exposed to the QCM-D sensors (arrow 1) for 20 minutes, followed by rinsing with 100 mM NaCl solution (arrow 2).

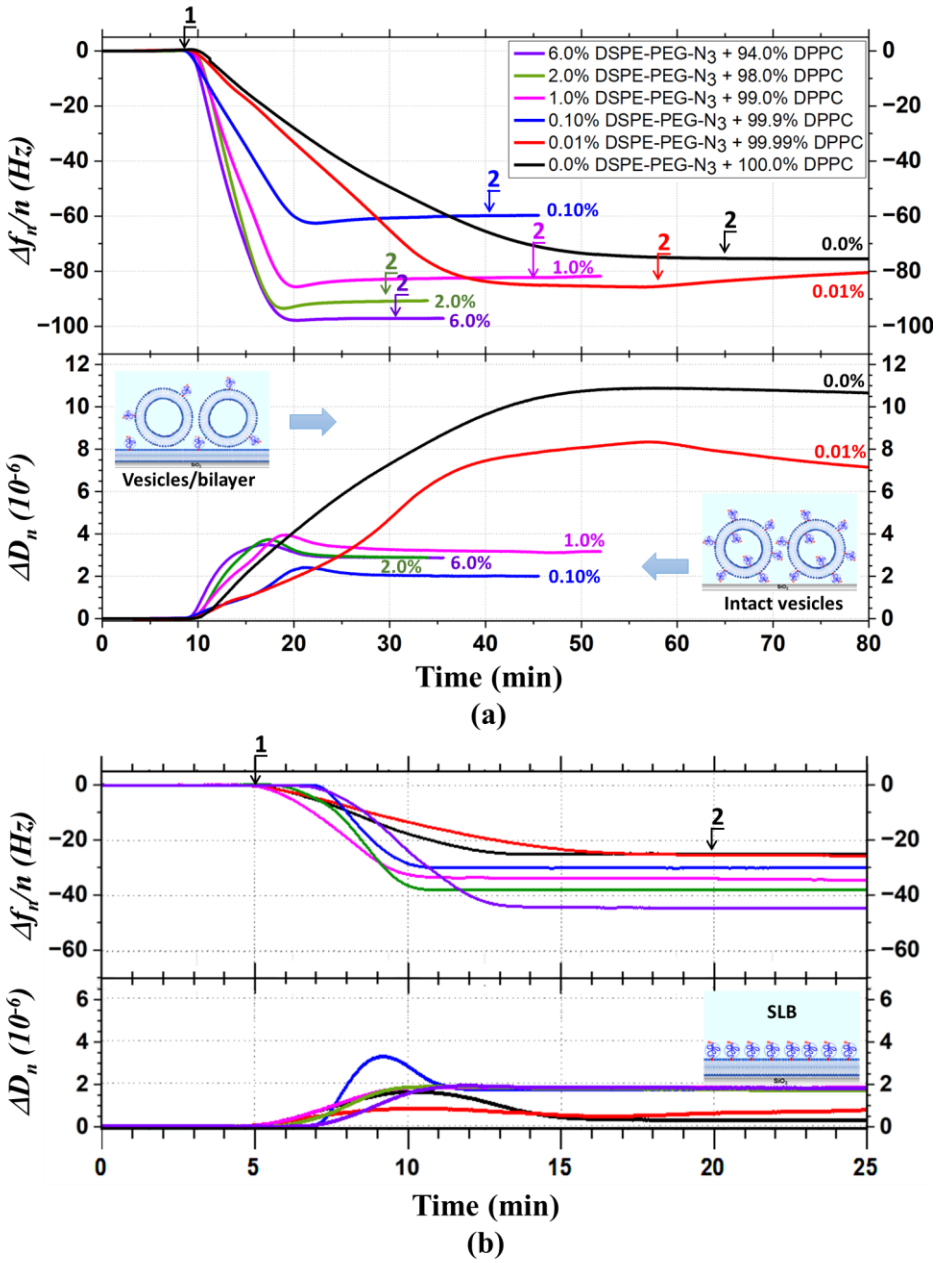

Figure 2. (a) QCM-D traces of $\Delta f_n/n$ *(n=3) and* ΔD_n vs time for exposure of SiO_2-coated crystals to DPPC (black curves) or DPPC + DSPE-PEG-N_3 (colored curves for different mol% DSPE-PEG-N_3 concentrations) vesicles at 21 °C. (b) Traces of $\Delta f_n/n$ *(n=7) and* ΔD_n vs time for exposure of SiO_2-coated crystals to DPPC (black curves) or DPPC + DSPE-PEG-N_3 (colored curves for different mol% DSPE-PEG-N_3 concentrations) vesicles at 50 °C. After a baseline (both $\Delta f_n/n$ *and* ΔD_n = 0) was established using 100 mM NaCl solution (flow rate = 20 µL/min). SiO_2-coated sensors were exposed to each vesicle solution (arrow 1), followed by rinsing with 100 mM NaCl solution (arrow 2).

Table 1. Deposit areal mass, thickness, average distance, area per lipid (APL), grafting density, reduced tethered density of DSPE-PEG-N_3 lipids in supported lipid bilayers (SLBs) formed by DPPC/DSPE-PEG-N_3 vesicles at 50°C.

Vesicle	**Supported lipid bilayer/SiO_2**						
mol% DSPE-PEG-N_3	Deposited mass[a] (ng/cm^2)	DSPE-PEG-N_3					Thickness[d] (h, nm)
		mol% DSPE-PEG-N_3[b]	Distance[b] (l, nm)	APL[b] (nm^2)	Grafting density[b] (σ, chains/nm^2)	Reduced tethered density[c] (Σ,chains)	
6	807.5 ± 12.1	28.1	0.98	1.0	1.04	7.4	10.0
2	691.4 ± 18.9	19.0	1.2	1.4	0.70	4.9	9.7
1	642.8 ± 30.3	15.2	1.3	1.8	0.56	3.9	8.5
0.1	555.3 ± 25.9	8.3	1.8	3.3	0.31	2.2	6.0
0.01	465.4 ± 10.9	1.3	4.6	21.2	0.05	0.3	5.8
0	449.1 ± 5.0	0	NA	NA	NA	NA	4.5

[a]Deposited mass of elastic SLB ($\Delta D_n < 2.0 \times 10^{-6}$) determined using the Sauerbrey equation[38-47] for final $\Delta f_n/n$ ($n=3,5,7$) values (Figure S5, SI); [b]mol%, distance, APL, and grafting density of DSPE-PEG-N_3 in the lipid bilayers were determined analytically using methods described in detail in the supplement (Supporting Information; Table S4); [c]Reduced tethered density (Σ) determined by using $\Sigma = \sigma\ \pi\ Rg^2$ where radius of gyration (R_g) of free PEG (M_w = 2000, in D_2O) is ~1.5 nm,[52,53]and σ is the grafting density of DSPE-PEG-N_3; [d]Thickness determined by modeling experimental curves for $\Delta f_n/n$ ($n=3,5,7$) and ΔD_n vs time using a Voigt viscoelastic model[40-47] (Figures S5, SI).

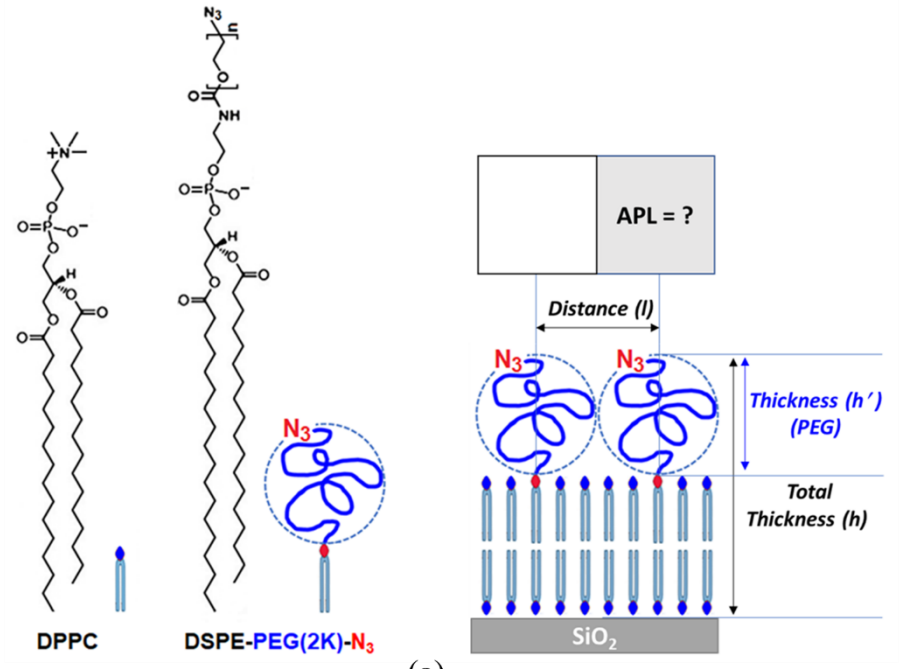

(a)

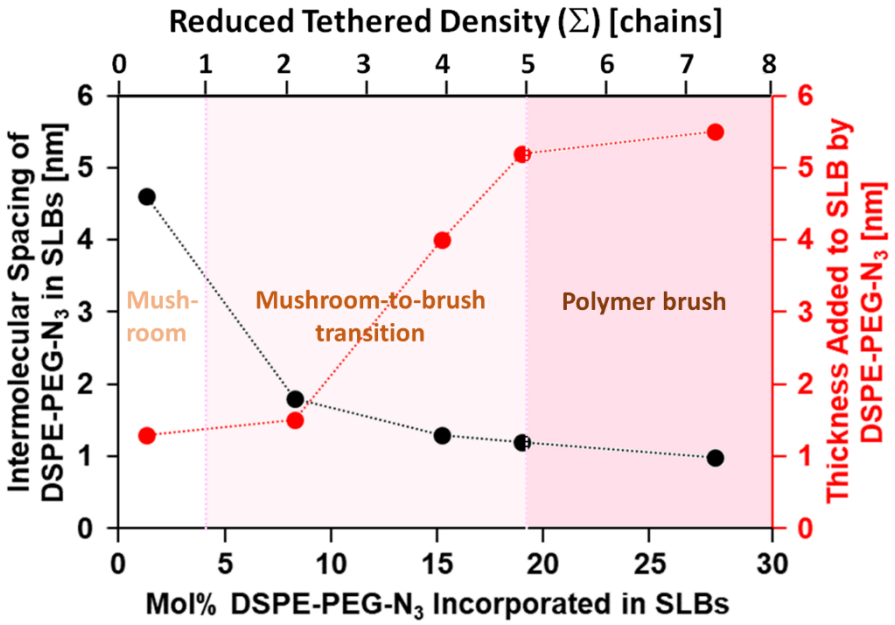

(b)

Figure 3. (a) Schematic representation of DPPC supported lipid bilayer (SLB) blended with DSPE-PEG-N_3 (PEG, M_w = 2000). Radius of gyration (R_g) of free PEG (M_w = 2000, in D_2O) = ~1.5 nm.[52,53] (b) The intermolecular spacing (*l,* nm) and reduced tethered density (Σ) of DSPE-PEG-N_3 in the SLBs, and thickness increase (*h', nm*) due to the addition of DSPE-PEG-N_3 is given as a function of mol% DSPE-PEG-N_3.

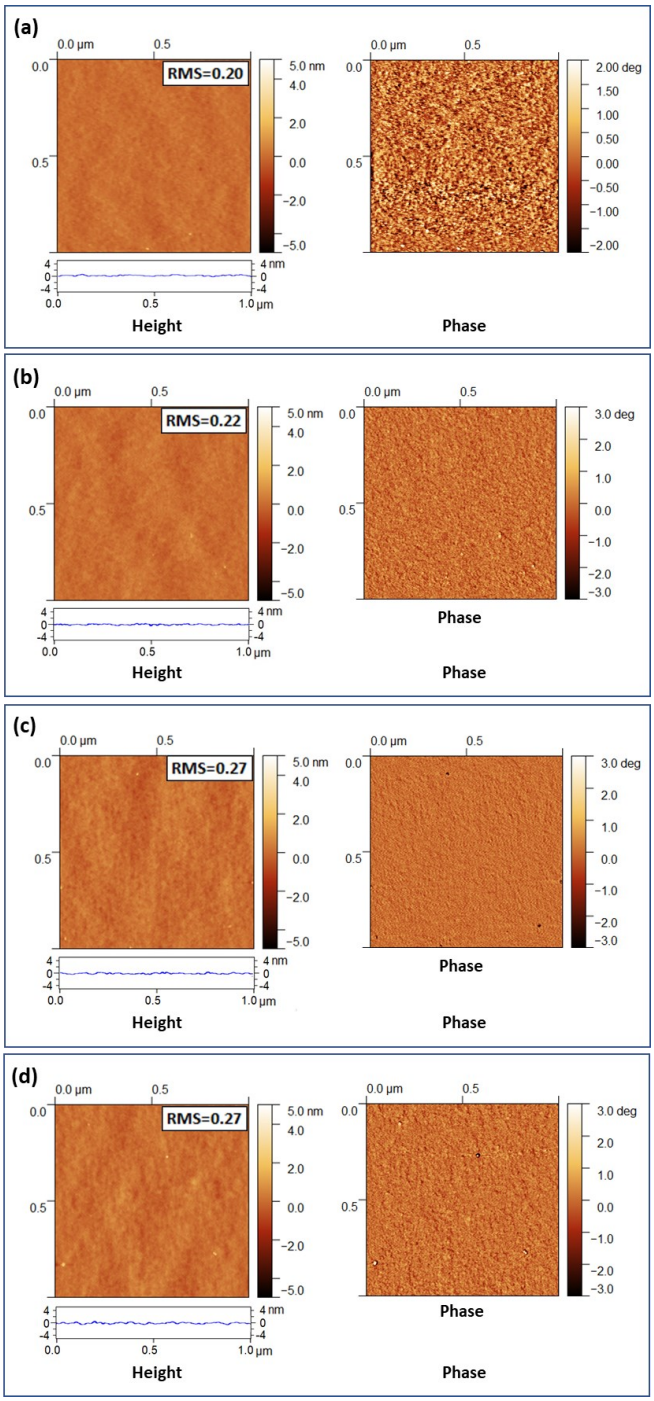

Figure 4. AFM images of SiO_2 surfaces after DPPC/DSPE-PEG-N_3 SLB deposition at 50 °C. (a) SiO_2 surface alone. (b) SLB formed using 100% DPPC vesicles. (c) SLB formed using DPPC+0.01% DSPE-PEG-N_3 vesicles. (d) SLB formed using DPPC+1.0% DSPE-PEG-N_3 vesicles. Left most panels indicate height and rightmost panels indicate phase. The blue lines represent line scans shown below each AFM image. RMS represents the root-mean-square roughness (R_{rms}) of the corresponding surface in nm.

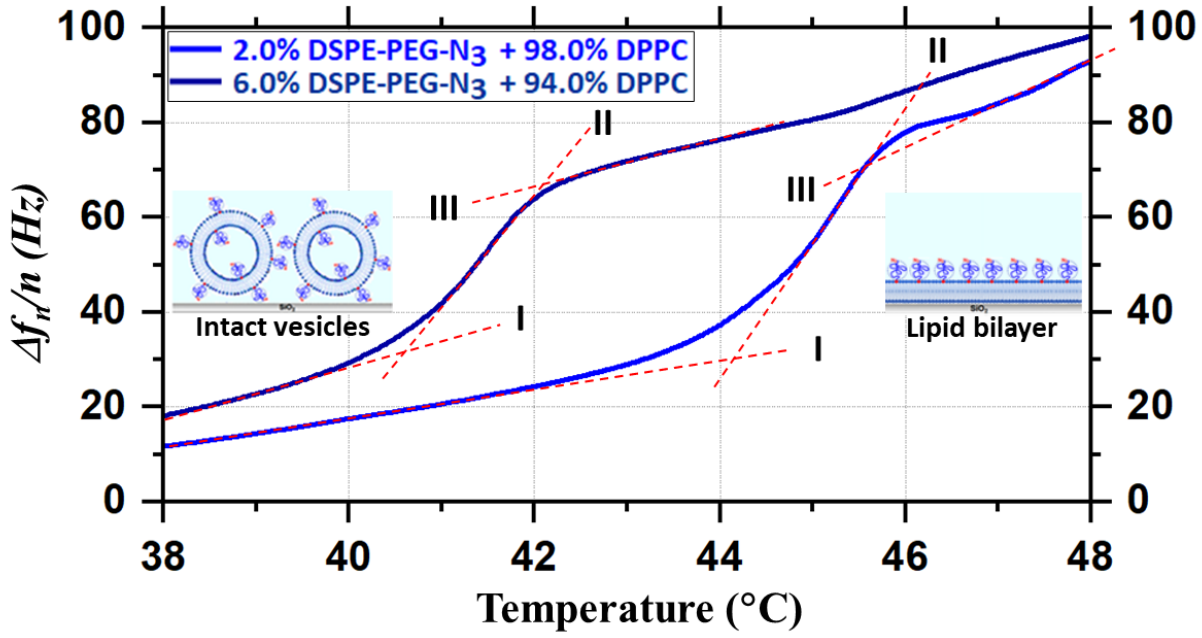

Figure 5. Traces of $\Delta f_n/n$ $(n=7)$ vs temperature (°C) for layers of DPPC/DSPE-PEG-N_3 vesicles containing either 2.0 mol% or 6.0 mol% DSPE-PEG-N_3, adsorbed on SiO_2 coated crystal. After forming layers of intact vesicles at 21°C (flow rate = 20 µL/min), the temperature was increased from 21°C to 50°C at the same flow rate (Figure S6 in the supporting information**)**. Stage I: Thermal variation of intact vesicles. Stage II: Mass loss for the two layers starts at 42 and 40 °C, respectively, as intact vesicles rupture to form SLBs. Stage III: Thermal variation of SLBs.

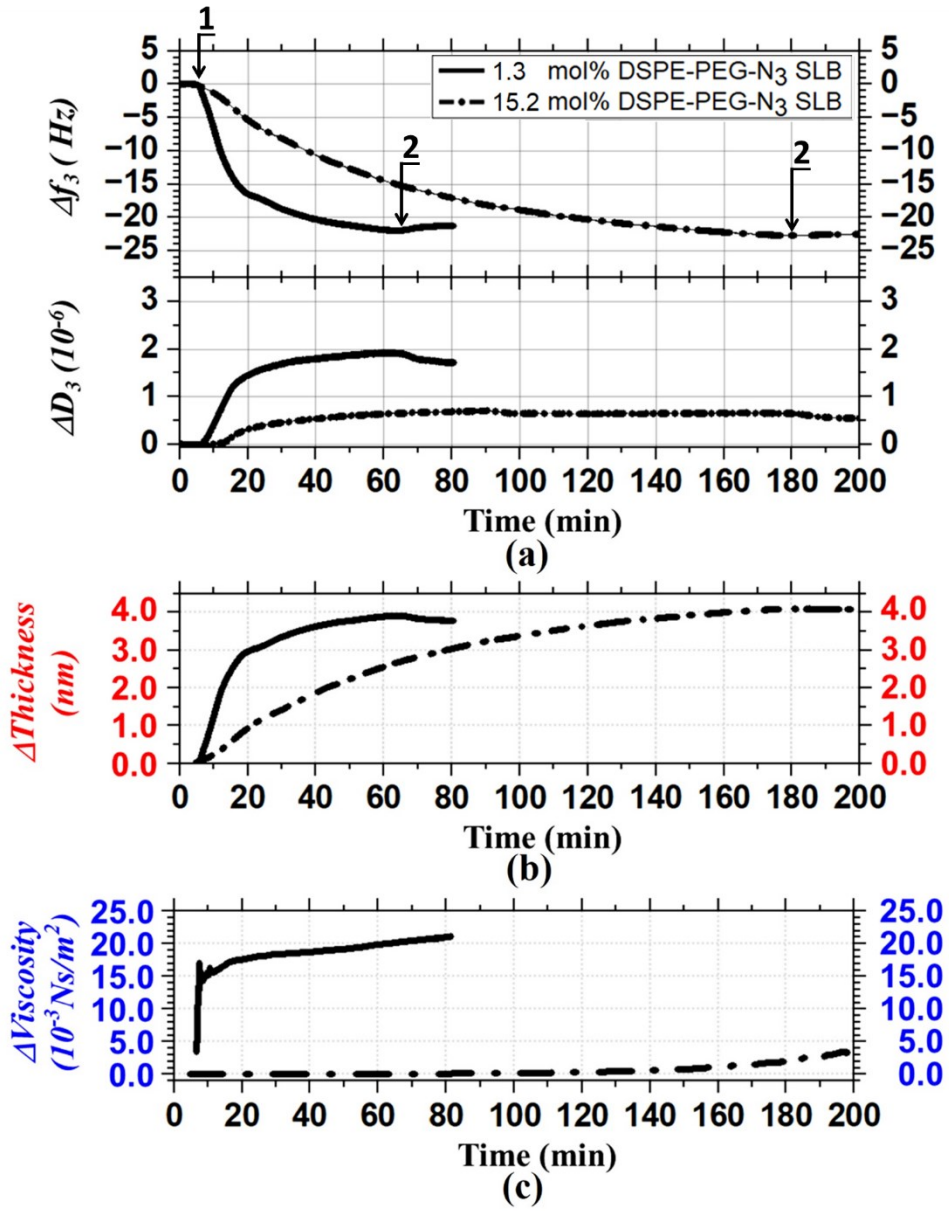

Figure 6. (a) Traces of $\Delta f_3/3$ and ΔD_3 versus time for DBCO-IgG grafting to azide-end-functionalized SLBs containing 1.3 mol% and 15.2 mol% of DSPE-PEG-N_3, respectively. After using 100 mM NaCl solution to establish a baseline at 30 °C (flow rate = 10 µL/min), each azide-functionalized SLBs on SiO_2-coated QCM crystal sensors were exposed to DBCO-functionalized IgG solution at arrow 1, followed by rinsing with 100 mM NaCl solution at arrow 2. (b) Each thickness change versus time and (c) each viscosity change versus time was determined by fitting experimental curves for $\Delta f_n/n$ $(n=3,5,7)$ and ΔD_n vs time, to a Voigt viscoelastic model (see Figure S9).

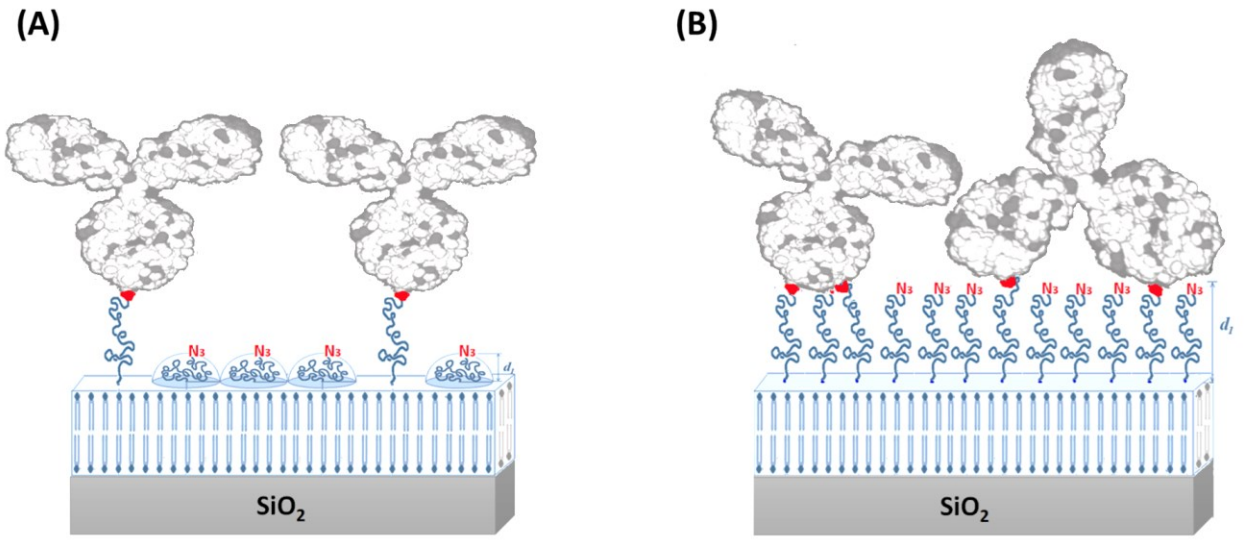

Figure 7. Schematic representation of DBCO (20x) IgG grafted onto azide-functionalized SLBs containing (A) 1.3 mol% and (B) 15.2 mol% DSPE-PEG-N_3. IgG images were modified from the structure of immunoglobulin G and lysine.[55] Gray regions (●) of IgG represent DBCO functional groups whereas red (●) represents conjugation of DBCO on IgG with N_3 tethered to the extended PEG chain.

Table 2. The thickness and viscosity changes for DBCO (20x)-IgG grafted to azide-end functionalized SLBs.

N_3-end functionalized SLBs on SiO_2 (at 50 °C)[a]			**DBCO (20x)-IgG grafted to SLBs on SiO_2 (at 30 °C)**				
mol% DSPE-PEG-N_3	Distance (*l, nm*)	Thickness (*h, nm*)	*Final $\Delta f_3/3$ (Hz)*	*Final ΔD_3 (10^{-6})*	*ΔThickness[b] (nm)*	*ΔViscosity[b] (10^{-3}Ns/m^2)*	Chemical Grafting
0 (control)	NA	4.5	~0	~0	NA	NA	No
1.3	4.6	5.8	-18	1.8	3.8	24.5	Yes
15.2	1.3	8.5	-22	0.7	4.8	3.75	Yes

[a]Azide-end functionalized SLBs formed from vesicles using DPPC, DPPC+0.01 mol% DSPE-PEG-N_3, and DPPC+1.0 mol% DSPE-PEG-N_3. [b]Thickness and viscosity was determined by modeling experimental curves for $\Delta f_n/n$ ($n=3,5,7$) and ΔD_n vs. time using a Voigt viscoelastic model (see Figure S9, SI).

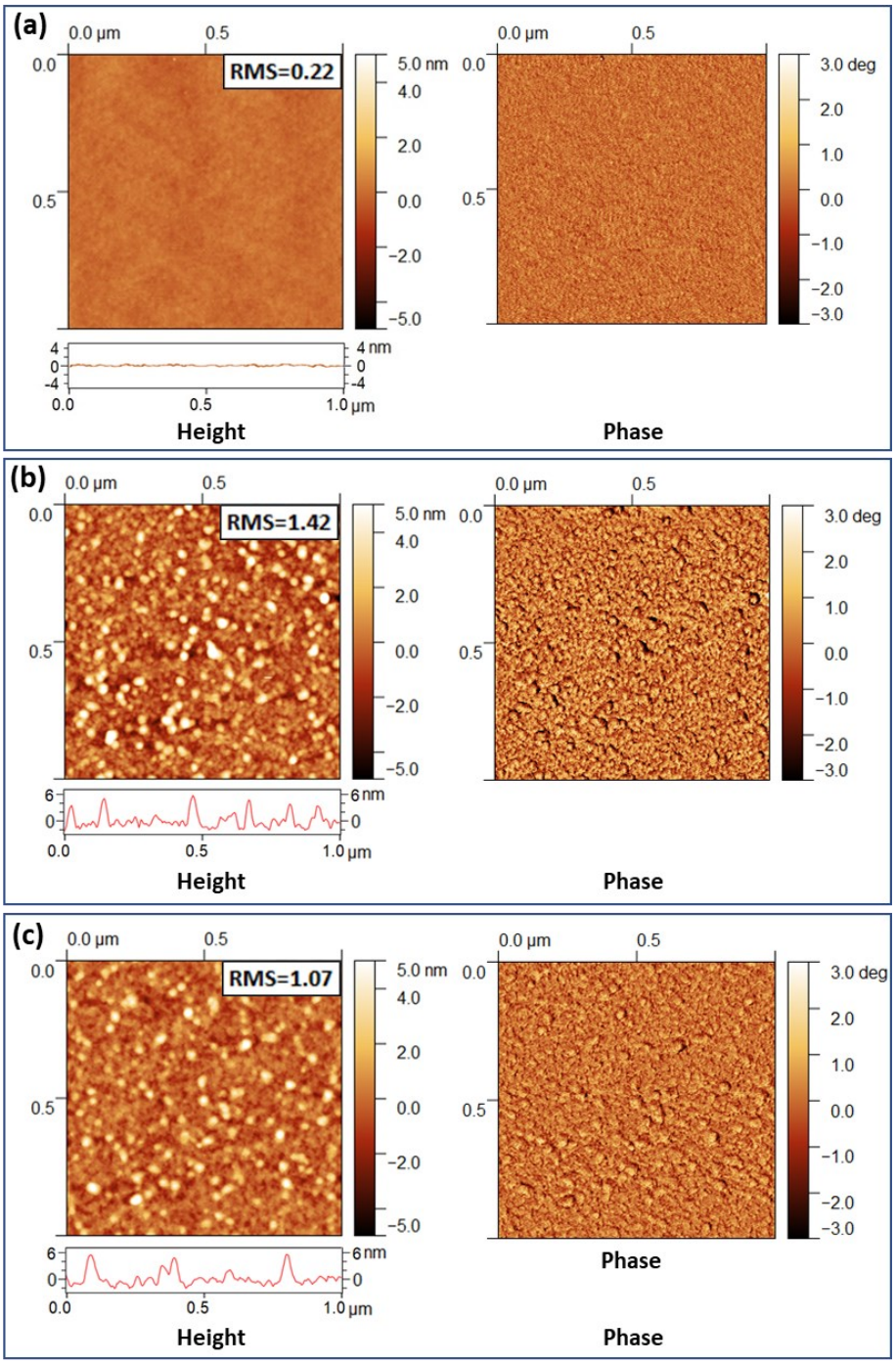

Figure 8. (a) AFM images of an SiO_2 surface after deposition of a pure DPPC SLB bilayer, then exposure to DBCO-IgG. (b) and (c) AFM images of SiO_2 surfaces after deposition of azide-end-functionalized SLBs containing (b) 1.3 mol% and (c) 15.2 mol% DSPE-PEG-N_3, respectively, then exposure to DBCO-IgG at 30 °C. Left most panels indicate height and rightmost panels indicate phase. The red lines represent line scans shown below each AFM image. RMS represents the root-mean-square roughness (R_{rms}) of the corresponding surface in nm.

Supporting Information.

This material is available free of charge via the Internet at http://pubs.acs.org.

AUTHOR INFORMATION

Corresponding Authors

*E-mail: leeh1@seas.upenn.edu (H.-S.L)

*E-mail: myerson@pennmedicine.upenn.edu (J.W.M.)

*E-mail: composto@seas.upenn.edu (R.J.C.)

Credit authorship contribution statement

Hyun-Su Lee: Formal analysis, Investigation, Writing – original draft, Writing – review & editing. **Ye Chan Kim:** Formal analysis, Investigation. **Jacob S. Brenner:** Supervision, Writing – review & editing. **Vladimir R. Muzykantov:** Supervision, Writing – review & editing. **Jacob W. Myerson:** Formal analysis, Investigation, Project administration, Writing – review & editing. **Russell J. Composto:** Conceptualization, Formal analysis, Investigation, Project administration, Writing – review & editing.

ORCID

Hyun-Su Lee: 0000-0002-5245-8430

Ye Chan Kim: 0000-0002-5122-9716

Jacob S. Brenner: 0000-0001-8437-0161

Vladimir R. Muzykantov:

Jacob W. Myerson

Russell J. Composto: 0000-0002-5906-2594

Declaration of Competing Interest

The authors declare that they have no known competing financial interests or personal relationships that could have appeared to influence the work reported in this paper.

ACKNOWLEDGMENT

R.J.C. acknowledges funding from NSF/DMR Polymers Program, DMR1905912, and NSF/CBET2034122 (RJC). V.R.M., J.S.B, and J.W.M. acknowledge funding from NIH R01 HL157189. Supported in part by the Institute for Translational Medicine and Therapeutics of the Perelman School of Medicine at the University of Pennsylvania (JWM, HSL, RJC). Research reported in this publication was supported by the National Center for Advancing Translational Sciences of the National Institutes of Health under Award Number UL1TR001878. The content is solely the responsibility of the authors and does not necessarily represent the official views of the NIH. Work was also supported by the Health Research Formula Fund financed by the PA State Grant (VRM, JSB, JWM, RJC, HSL). R.J.C. acknowledges facility support from MRSEC-DMR-1720530 and facility assistance from Dr. Matt Brukman from the Nanoscale Characterization Facility. This research used resources from the University of Pennsylvania's Nanoscale Characterization Facility, an NNCI member supported by NSF ECCS-1542153 and by NSF MRSEC-DMR-1720530. We gratefully acknowledge use of QCM-D in the laboratory of Professor. D. Lee.

REFERENCES

(1) Zhou, F.; Pan, W.; Chang, Y.; Su, X.; Duan, X.; Xue, Q. A Supported Lipid Bilayer-Based Lab-on-a-Chip Biosensor for the Rapid Electrical Screening of Coronavirus Drugs. ACS Sens. 2022, 7 (7), 2084–2092.

(2) Lubrano, C.; Matrone, G. M.; Iaconis, G.; Francesca Santoro, F. New Frontiers for Selective Biosensing with Biomembrane-Based Organic Transistors ACS Nano 2020, 14(10), 12271–12280.

(3) Costello, D. A.; Millet, J. K.; Hsia,C. -Y.; Whittaker, G. R.; Daniel, S. Single particle assay of coronavirus membrane fusion with proteinaceous receptor-embedded supported bilayers. Biomaterials 2013, 34(32), 7895-7904.

(4) Bally, M.; Graule, M.; Parra, F.; Larson, G.; Höök, F. A virus biosensor with single virus-particle sensitivity based on fluorescent vesicle labels and equilibrium fluctuation analysis. Biointerphases 2013, 8, 4.

(5) Khorshid, M.; Losada-Pérez, P.; Wackers, G.; Yongabi, D.; Renner, F. U.; Thoelen, R.; Wagner, P. Real-time monitoring of interactions between Ebola fusion peptide and solid-supported phospholipid membranes: Effect of peptide concentration and layer geometry. Phys. Med. 2017, 4, 1– 7.

(6) Heider, S.; Reimhult, E.; Metzner, C. Real-time analysis of protein and protein mixture interaction with lipid bilayers. Biochim. Biophys. Acta, Biomembr. 2018, 1860, 319–328.

(7) Yu, X.; Xia, Y.; Tang, Y.; Zhang, W.-L.; Yeh, Y.-T.; Lu, H.; Zheng, S.-Y. A Nanostructured Microfluidic Immunoassay Platform for Highly Sensitive Infectious Pathogen Detection. 2017, 12, 1700425.

(8) Di Iorio, D.; Verheijden, M. L.; Van Der Vries, E.; Jonkheijm, P.; Huskens, J. Weak Multivalent Binding of Influenza Hemagglutinin Nanoparticles at a Sialoglycan-Functionalized Supported Lipid Bilayer. ACS Nano 2019, 13, 3413– 3423.

(9) Toyoda, Y.; Morimoto, K.; Suno, R.; Horita, S.; Yamashita, K.; Hirata, K.; Sekiguchi, Y.; Yasuda, S.; Shiroishi, M.; Shimizu, T.; Urushibata, Y.; Kajiwara, Y.; Inazumi, T.; Hotta, Y.; Asada, H.; Nakane, T.; Shiimura, Y.; Nakagita, T.; Tsuge, K.; Yoshida, S.; Kuribara, T.; Hosoya, T.; Sugimoto, Y.; Nomura, N.; Sato, M.; Hirokawa, T.; Kinoshita, M.; Murata, T.; Takayama, K.; Yamamoto, M.; Narumiya, S.; Iwata, S.; Kobayashi, T. Ligand binding to human prostaglandin E receptor EP 4 at the lipid-bilayer interface. Nat. Chem. Biol. 2019, 15, 18– 26.

(10) Wu, J. C.; Tseng, P. Y.; Tsai, W. S.; Liao, M. Y.; Lu, S. H.; Frank, C. W.; Chen, J. S.; Wu, H. C.; Chang, Y. C. Antibody conjugated supported lipid bilayer for capturing and purification of viable tumor cells in blood for subsequent cell culture. Biomaterials 2013, 34, 5191– 5199.

(11) Yeh, P. Y.; Chen, Y. R.; Wang, C. F.; Chang, Y. C. Promoting Multivalent Antibody-Antigen Interactions by Tethering Antibody Molecules on a PEGylated Dendrimer-Supported Lipid Bilayer. Biomacromolecules 2018, 19, 426– 437.

(12) Zhang, J.; Wang, X.; Chen, T.; Feng, C.; Li, G. Electrochemical Analysis of Enzyme Based on the Self-Assembly of Lipid Bilayer on an Electrode Surface Mediated by Hydrazone Chemistry. Anal. Chem. 2017, 89, 13245– 13251.

(13) Hartley, M. D.; Schneggenburger, P. E.; Imperiali, B. Lipid bilayer nanodisc platform for investigating polyprenol-dependent enzyme interactions and activities. Proc. Natl. Acad. Sci. U. S. A. 2013, 110, 20863– 20870.

(14) Shang, J.; Ye, G.; Shi, K.; Wan, Y.; Luo, C.; Aihara, H.; Geng, Q.; Auerbach, A.; Li, F. Structural basis of receptor recognition by SARS-CoV-2. Nature 2020, 581, 221– 224.

(15) Hamming, I.; Timens, W.; Bulthuis, M. L. C.; Lely, A. T.; Navis, G. J.; van Goor, H. Tissue distribution of ACE2 protein, the functional receptor for SARS coronavirus. A first step in understanding SARS pathogenesis. J. Pathol. 2004, 203, 631– 637.

(16) Walls, A. C.; Park, Y. J.; Tortorici, M. A.; Wall, A.; McGuire, A. T.; Veesler, D. Structure, Function, and Antigenicity of the SARS-CoV-2 Spike Glycoprotein. Cell 2020, 181, 281– 292 e6.

(17) Kuo, C.-J.; Chiang, H.-C.; Tseng, C.-A.; Chang, C.-F.; Ulaganathan, R. K.; Ling, T.-T.; Chang, Y.-J.; Chen, C.-C.; Chen, Y.-R.; Chen, Y.-T. Lipid-Modified Graphene-Transistor Biosensor for Monitoring Amyloid-β Aggregation. ACS Appl. Mater. Interfaces 2018, 10, 12311– 12316.

(18) Howard, M.; Zern, B. J.; Anselmo, A. C.; Shuvaev, V. V.; Mitragotri, S.; Muzykantov, V. Vascular Targeting of Nanocarriers: Perplexing Aspects of the Seemingly Straightforward Paradigm. *ACS Nano* 2014, 8, 5, 4100–4132.

(19) Glassman, P. M.; Myerson, J. W.; Ferguson, L. T.; Kiseleva, R. Y.; Shuvaev, V. V.; Jacob S. Brenner, J. S.; Muzykantov, V. R. Targeting drug delivery in the vascular system: Focus on endothelium. *Adv. Drug Deliv. Rev.,* 2020, 157, 96-117.

(20) Parhiz, H.; Shuvaev, V. V.; Pardi, N.; Khoshnejad, M.; Kiseleva, R. Y.; Jacob S. Brenner, J. S.; Uhler, T.; Tuyishime, S.; Mui, B. L.; Tam, Y. K.; Madden, T. D.; Hope, M. L.; Weissman, D.; Muzykantov, V. R. PECAM-1 directed re-targeting of exogenous mRNA providing two orders of magnitude enhancement of vascular delivery and expression in lungs independent of apolipoprotein E-mediated uptake. *J. Control. Release* 2018, 291, 106-115.

(21) Cheng, Z.; Al Zaki, A.; Hui, J. Z.; Muzykantov, V. R.; Tsourkas, A. Multifunctional Nanoparticles: Cost Versus Benefit of Adding Targeting and Imaging Capabilities. *Science,* 2012, 338, 903-910.

(22) Myerson, JW; Patel, PN; Rubey, KM; Zamora, ME; Zaleski, MH; Habibi, N; Walsh, LR; Lee, Y-W; Luther, DC; Ferguson, LT; Marcos-Contreras, OA; Glassman, PM; Mazaleuskaya, LL; Johnston, I; Hood, ED; Shuvaeva, T; Wu, J; Zhang, H-Y; Gregory, JV; Kiseleva, RY; Nong, J; Grosser, T; Greineder, CF; Mitragotri, S; Worthen, GS; Rotello, VM; Lahann, J; Muzykantov, VR; Brenner JS (2022) Supramolecular arrangement of protein in nanoparticle structures predicts nanoparticle tropism for neutrophils in acute lung inflammation. Nature Nanotechnology, 17, 86-97.

(23) Wang Z; Brenner JS (2021) The Nano-War Against Complement Proteins. AAPS Journal 23(5): 105

(24) Wang, Z; Hood, ED; Nong, J; Ding, J; Marcos-Contreras, OA; Glassman, PM; Rubey, KM; Zaleski, M; Espy, CL; Gullipali, D; Miwa, T; Muzykantov, VR; Song, W-C; Myerson, JW; Brenner, JS (2021) Combating Complement's Deleterious Effects on Nanomedicine by Conjugating Complement Regulatory Proteins to Nanoparticles. Advanced Materials, 34 (8) 2107070.

(25) Richter, R.; Mukhopadhyay, A.; Brisson, A. Pathways of Lipid Vesicle Deposition on Solid Surfaces: A Combined QCM-D and AFM Study. Biophys J. 2003, 85(5), 3035–3047.

(26) Keller, C. A.; Kasemo, B. Surface specific kinetics of lipid vesicle adsorption measured with a quartz crystal microbalance. Biophys. J. 1998, 75, 1397–1402.

(27) Reimhult, E.; Höök, F.; Kasemo, B. Vesicle adsorption on SiO2 and TiO2: dependence on vesicle size. J. Chem. Phys. 2002, 117, 7401–7404.

(28) Bibissidis, N.; Betlem, K.; Cordoyiannis, G.; Prista-von Bonhorst, F.; Goole, J.; Raval, J.; Daniel, M.; Góźdź, W.; Iglič, A.; Losada-Pérez, P. Correlation between adhesion strength and phase behaviour in solid-supported lipid membranes. J. Mol. Liq. 2020, 320, 114492.

(29) Reviakine, I.; Brisson, A. Formation of supported phospholipid bilayers from unilamellar vesicles investigated by atomic force microscopy. Langmuir. 2000, 16, 1806–1815.

(30) Zhdanov, V. P.; Kasemo, B. Comments on rupture of adsorbed vesicles Langmuir, 2001, 17, 3518-3521.

(31) Zhdanov, V. P.; Keller, C. A.; Glasmästar, K.; Kasemo, B. Simulation of adsorption kinetics of lipid vesicles J. Chem. Phys., 2000, 112, 900-909.

(32) Seifert, U. Configuration of fluid membranes and vesicles. Adv. Phys., 1997, 46, 13-137

(33) Lind, T. K.; Cárdenas, M.; Wacklin, H. P. Formation of Supported Lipid Bilayers by Vesicle Fusion: Effect of Deposition Temperature. Langmuir 2014, 30, 7259−7263.

(34) Cho, N. -J; Jackman, J. A.; Liu, M.; Frink, C.W. pH-Driven Assembly of Various Supported Lipid Platforms: A Comparative Study on Silicon Oxide and Titanium Oxide. Langmuir 2011, 27, 7, 3739–3748.

(35) Tabaei, S. R.; Choi, J. -H.; Zan, G. H.; Zhdanov, V. P.; Cho, N. -J. Solvent-Assisted Lipid Bilayer Formation on Silicon Dioxide and Gold. Langmuir 2014, 30, 34, 10363–10373.

(36) Tucker Andrews, J.; Baker, K. E.; Handloser, J. T.; Bridges, N.; Krone; A. A.; Kett, P. J. N. Formation of Supported Lipid Bilayers (SLBs) from Buffers Containing Low Concentrations of Group I Chloride Salts. Langmuir 2021, 37, 44, 12819–12833.

(37) Tae, H.; Yang, C.; Cho, N. -J. Artificial Cell Membrane Platforms by Solvent-Assisted Lipid Bilayer (SALB) Formation. Acc. Mater. Res. 2022, 3, 12, 1272–1284.

(38) Sauerbrey, G. The use of quartz oscillators for weighing thin layers and for microweighing. Z. Phys. 1959, 155, 206-222.

(39) Vogt, B. D.; Lin, E. K.; Wu, W. L.; White, C. C. Effect of Film Thickness on the Validity of the Sauerbrey Equation for Hydrated Polyelectrolyte Films. J. Phys. Chem. B 2004, 108 (34), 12685-12690.

(40) Lee, H. -S.; Penn, L. S. In Situ Study of Polymer Brushes as Selective Barriers to Diffusion. Macromolecules 2008, 41 (21), 8124-8129.

(41) Lee, H. -S.; Penn, L. S. Evidence for Relative Radius of Gyration as the Criterion for Selective Diffusion Behavior of Polymer Brushes. Langmuir 2009, 25 (14), 7983-7989.

(42) Lee, H. -S.; Dastgheyb, S. S.; Hickok, N. J.; Eckmann, D. M.; Composto, R. J. Targeted Release of Tobramycin from a pH-Responsive Grafted Bilayer Challenged with S. aureus. Biomacromolecules 2015, 16 (2), 650-659.

(43) Hook, F.; Kasemo, B.; Nylander, T.; Fant, C.; Sott, K.; Elwing, H. Variations in coupled water, viscoelastic properties, and film thickness of a Mefp-1 protein film during adsorption and cross-linking: A quartz crystal microbalance with dissipation monitoring, ellipsometry, and surface plasmon resonance study. Anal. Chem. 2001, 73 (24), 5796-5804.

(44) Lee, H. -S.; Yee, M. Q.; Eckmann, Y. Y.; Hickok, N. J.; Eckmann, D. M.; Composto, R. J. Reversible swelling of chitosan and quaternary ammonium modified chitosan brush layers: effects of pH and counter anion size and functionality. J. Mater. Chem. 2012, 22, 19605-19616.

(45) Lee, H. -S.; Eckmann, D. M.; Lee, D. Y.; Hickok, N. J.; Composto, R. J. Symmetric pH-Dependent Swelling and Antibacterial Properties of Chitosan Brushes. Langmuir 2011, 27 (20), 12458-12465.

(46) Lee, H. -S.; Myers, C.; Zaidel, L.; Nalam, P. C.; Caporizzo, M. A.; Daep, C. A.; Eckmann, D. M.; Masters, J. G.; Composto, R. J. Competitive Adsorption of

Polyelectrolytes onto and into Pellicle-Coated Hydroxyapatite Investigated by QCM-D and Force Spectroscopy. ACS Appl. Mater. Interfaces 2017, 9, 15, 13079–13091.

(47) Lee, H. -S.; Tsai, S.; Kuo, C.; Bassani, A.; Pepe-Mooney, B.; Miksa, D.; Masters, J.; Sullivan, R.; Composto, R. J. Chitosan Adsorption on Hydroxyapatite and its Role in Preventing Acid Erosion. Journal of Colloid and Interface Science 2012, 385, 235-243.

(48) Chaban, V. Computationally efficient prediction of area per lipid. Chemical Physics Letters 2014, 616–617, 25–29.

(49) Gu, R. X.; de Groot, B.L. Lipid-protein interactions modulate the conformational equilibrium of a potassium channel. *Nat Commun* 2020, 11, 2162.

(50) Lochbaum, C. A.; Chew, A. K.; Zhang, X.; Rotello, V.; Van Lehn, R. C.; Pedersen, J. A. Lipophilicity of Cationic Ligands Promotes Irreversible Adsorption of Nanoparticles to Lipid Bilayers. *ACS Nano* 2021, 15, 6562−6572.

(51) Li, M.; Jiang, S.; Simon, J.; Paßlick, D.; Frey, M.-L.; Wagner, M.; Mailänder, V.; Crespy, D.; Landfester, K. Brush Conformation of Polyethylene Glycol Determines the Stealth Effect of Nanocarriers in the Low Protein Adsorption Regime. Nano Lett. 2021, 21, 1591– 1598.

(52) Lee, H.; de Vries, A. H.; Marrink, S. -J.; Pastor, R. W. A Coarse-Grained Model for Polyethylene Oxide and Polyethylene Glycol: Conformation and Hydrodynamics. J. Phys. Chem. B 2009, 113, 13186–13194.

(53) Rubinson, K.N.; Krueger, S. Poly(ethylene glycol)s 2000–8000 in water may be planar: A small-angle neutron scattering (SANS) structure study. Polymer 2009, 50, 4852–4858.

(54) Brittain, W. J.; Minko, S. A Structural Definition of Polymer Brushes. *J. Polym. Sci., Part A: Polym. Chem.* 2007, 45(16), 3505–3512.

(55) Tan, Y. H.; Liu, M.; Nolting, B.; Go, J. G.; Gervay-Hague, J.; Liu, G. A Nanoengineering Approach for Investigation and Regulation of Protein Immobilization. *ACS Nano* 2008, 2 (11), 2374–2384.

Artwork and Tables with Captions